Numerical modeling of wave propagation in random anisotropic heterogeneous elastic media

Quang-Anh Ta, Didier Clouteau, Régis Cottereau

Numerical modeling of wave propagation in random anisotropic heterogeneous elastic media

Q.-A. Ta, D. Clouteau, R. Cottereau
Laboratoire MSSMat UMR 8579, École Centrale Paris, CNRS,
Grande voie des vignes, 92995 Châtenay-Malabry, France
e-mail: **regis.cottereau@ecp.fr**

Abstract

This paper describes some numerical experiments that were performed on wave propagation in a randomly generated anisotropic heterogeneous elastic media. By comparison with more classical, homogeneous media, several numerical issues arise that are presented in detail. In particular, an appropriate parameterization has to be chosen for the field of mechanical properties, and the Perfectly Matched Layers have to be modified for such media, lest the stability be lost. Some open questions will also be raised. Finally, we will present ongoing research on the characterization of the physical phenomena taking place over long distances depending on the type of random elasticity model used.

1   Introduction

The isotropic and homogeneous soil models commonly used for the propagation of waves in geophysical media are not compatible with the surface recordings available [2, 21, 19]. In particular, the coda of the seismic recordings cannot be reproduced with these simple models. It is therefore desirable to consider heterogeneous anisotropic media, but this possibility is hindered by several numerical difficulties that we address in this presentation.

The first issue concerns the parameterization of the properties of the medium. With a view at identification, this parameterization should at the same time ensure a sufficient heterogeneity, while retaining only a few parameters. Considering one realization (sample) of the random medium yields that goal and a random model of the elasticity tensor will be described in section 2. In that model, the elasticity tensor varies continuously in space, so that special integration schemes should be used within the context of Finite Elements. This point has been considered here only in a crude manner, considering a certain number of integration points per correlation length, after some numerical tests (not presented in this paper). Section 2 concentrates on the construction of the random model of the elasticity tensor, and on the generation of samples of this model. It is worth noticing that in this section only samples of random media will be considered and no real statistical analyses will be performed. However, since the elastic waves are traveling through a statistically homogeneous random media, the wave pattern obtained after several wavelengths and correlation lengths is expected to show common statistical properties weakly dependent on the sample of the random media. In particular, this property has been observed when considering the multiple scattering of seismic wave fields on a random distribution of buildings [9].

The next issue is that of wave propagation. Since the goal is to characterize the wave propagation pattern in a heterogeneous medium beyond the *mean free path*, a numerical method is required, that is able to account for several wavelengths and correlation lengths in all spatial directions. Moreover, since the multiple scattering pattern drastically changes between two and three dimensional cases, 3D simulations are targeted. In order to meet both a high efficiency and a controlled numerical error, the Spectral Finite Element Method has been chosen [1]. In particular, the SPEC software developed by the Seismology Group of *Institut de*

Physique du Globe de Paris [14] has been modified in order to account for anisotropic heterogeneous fields of elastic tensors. Besides the numerical scheme, it is also necessary to choose the type of absorbing boundary conditions of layers that should be used when the computational domain has to be limited. The Perfectly Matched Layers (PMLs) have reached a position of choice in the last decade for this type of problem, but suffer in some particular cases of anisotropic media from instability issues. Unfortunately, for the the type of heterogeneous anisotropic media that we are considering here, the instability eventually always appear so that some special treatment has to be applied. Section 3 will present the instability problem and the patch that we applied.

Finally, we will present in section 4 some attempts at characterizing the type of physics at work in the medium. In particular, we will try to identify the transition form a wave propagation phenomenon to a diffusion behavior. Although this is on-going work, the aim is to be able at some point to use expensive wave propagation models only where necessary and to use simpler diffusion models where possible. This would also require the introduction of appropriate coupling schemes that will not be discussed here. We finish this introduction by the description of the problem at hand and of some of the main notations of this paper.

We consider an unbounded elastic domain Ω, described by an elasticity tensor C, linking the stress tensor σ and the strain tensor ϵ, and the bulk density ρ_v. The elasticity tensor is *a priori* fully anisotropic. The strong formulation of the elastic wave propagation in this medium consists in solving the Navier equation for $\boldsymbol{u}$ $\forall t \in [0; T]$:

$$\mathbf{Div}\big(C(\boldsymbol{x})\epsilon(\boldsymbol{u}(\boldsymbol{x}; t))\big) + \boldsymbol{f}(\boldsymbol{x}, t) = \rho_v \frac{\partial^2}{\partial t^2} \boldsymbol{u}(\boldsymbol{x}; t) \tag{1}$$

together with proper boundary and initial conditions. As far as the Spectral Finite Element Method is concerned, the related weak formulation is considered: find $\boldsymbol{u} \in V(\Omega)$, $\forall t \in [0; T]$, such that, $\forall \boldsymbol{w} \in V(\Omega)$:

$$\int_\Omega \left(\rho_v \frac{\partial^2 \boldsymbol{u}}{\partial t^2}(t) \cdot \boldsymbol{w} + C^*(\boldsymbol{x})\epsilon(\boldsymbol{u}(t)) : \epsilon(\boldsymbol{w}) - \boldsymbol{f}(\boldsymbol{x}, t) \cdot \boldsymbol{w} \right) d\Omega = 0. \tag{2}$$

In this weak formulation, Ω is separated into the computational domain of interest, in which the elasticity tensor $C^* = C$, and a PML domain in which the elasticity tensor is modified (see section 3), and $V(\Omega)$ is some appropriate functional space.

2 Random model of mechanical parameters

We first discuss the modeling issue. Indeed, experimental soil samples show a high level of heterogeneity, but on a given location, the data is usually far too scarce to identify a reasonable heterogeneous model of the mechanical parameters. The same issue is raised with respect to anisotropy, which is apparent in the available data but requires a large dataset to be identified appropriately. We propose here a stochastic model of the elasticity tensor of the soil that is both continuously heterogeneous and anisotropic [29, 30]. As it is random, its identification is based only on statistical quantities that are usually available over larger regions. Further the mean, the correlation lengths, and the level of anisotropy can be parameterized separately.

In subsection 2.1, we present a random model for a homogeneous elasticity tensor, with no variation in space. The main points are the introduction of two parameters, δ and δ_g, that control the anisotropy and variability levels in the medium. In subsection 2.2, we generalize it to the case of a random field of elasticity tensor, adding the variability in space through a model of correlation controlled by three correlation lengths. In the last subsection 2.3, we discuss the question of generating a sample of this random medium on a parallel computer.

2.1 Random elastic tensor

Using Voigt's notation, the 4-rank tensor of elasticity C can be represented by a 2-rank symmetric positive-definite matrix with 21 independent coefficients for general anisotropic materials. When the material shows

local symmetries the number of independent coefficients decreases and reduces to 2 independent coefficients in the isotropic case. Among other choices of that pair of coefficients, the tensor $\boldsymbol{C}^{iso}$ of an isotropic material can be written using the bulk modulus κ and shear modulus μ:

$$\boldsymbol{C}^{iso} = 3\kappa\boldsymbol{S} + 2\mu\boldsymbol{D} \tag{3}$$

where $\boldsymbol{S}$ and $\boldsymbol{D}$ are respectively the so-called *spherical* tensor and *deviatoric* tensor defined as: $\boldsymbol{S} = \frac{1}{3}\left(\mathbf{I_2} \otimes \mathbf{I_2}\right)$ and $\boldsymbol{D} = \mathbf{Id_6} - \boldsymbol{S}$ with $\mathbf{I_2} = [1\ 1\ 1\ 0\ 0\ 0]^{\mathrm{T}}$ and $\mathbf{Id_6}$ the identity matrix of $\mathbb{M}_6(\mathbb{R})$. Since $\{\boldsymbol{S}, \boldsymbol{D}\}$ are orthogonal projectors in the space of real symmetric matrices $\mathbb{M}_6^{\mathrm{s}}(\mathbb{R})$ ($\boldsymbol{S}^2 = \boldsymbol{S}$, $\boldsymbol{D}^2 = \boldsymbol{D}$ and $\boldsymbol{S}\boldsymbol{D} = 0$) and an orthogonal pair for the scalar product associated to the Frobenius norm ($\|\boldsymbol{S}\|_{\mathrm{F}} = 1$; $\|\boldsymbol{D}\|_{\mathrm{F}} = \sqrt{5}$), equation (3) also reads:

$$\boldsymbol{C}^{iso} = \left(\sqrt{3\kappa}\boldsymbol{S} + \sqrt{2\mu}\boldsymbol{D}\right)^2 \tag{4}$$

Based on equation (4), we propose to write a random anisotropic elasticity tensor as:

$$\boldsymbol{C}(\delta, \delta_g) = \left(\sqrt{3\kappa(\delta)}\boldsymbol{S} + \sqrt{2\mu(\delta)}\boldsymbol{D}\right)\boldsymbol{G}(\delta_g)\left(\sqrt{3\kappa(\delta)}\boldsymbol{S} + \sqrt{2\mu(\delta)}\boldsymbol{D}\right) \tag{5}$$

in which $\boldsymbol{G}(\delta_g)$, $\kappa(\delta)$ and $\mu(\delta)$ are random variables and (δ, δ_g) a pair of dispersion parameters. This model is detailed in sections (2.1.1-2.1.2).

2.1.1 The anisotropy kernel G

Following [29], the so-called anisotropy kernel $\boldsymbol{G}$ belongs to the set SG^+ of all normalized, symmetric, definite-positive real random matrices. This random variable is defined on the probability measure space $(\mathcal{A}, \mathcal{F}, P)$, with values in $\mathbb{M}_6^+(\mathbb{R})$, parameterized by a unique real positive dispersion parameter δ_g. According to [28], the construction by the maximization of the entropy [26, 17] leads to the following form of the kernel:

$$\boldsymbol{G}(\delta_g) = \boldsymbol{L}^{\mathrm{T}}(\delta_g)\boldsymbol{L}(\delta_g) \tag{6}$$

where $\boldsymbol{L}$ is an upper triangular matrix with entries defined as:

$$\boldsymbol{L}_{\mathrm{ij}}(\delta_g) = \begin{cases} \dfrac{\delta_g}{\sqrt{7}}\mathcal{G}_{\mathrm{k}}, & \text{for upper extra-diagonal entries j > i} \\ \dfrac{\delta_g}{\sqrt{7}}\sqrt{2h(\mathcal{G}_{\mathrm{k}}, \alpha_{\mathrm{i}})}, & \text{for diagonal entries j = i} \end{cases} \tag{7}$$

where:

- k is a reindexing : $\mathrm{k} = \frac{(14-\mathrm{i})(\mathrm{i}-1)}{2} + \mathrm{j} - \mathrm{i} + 1$

- $\mathcal{G}_{\mathrm{k}}$ for $\mathrm{k} = 1..21$ are 21 independent copies of a normalized centered Gaussian random variable $\mathcal{G}$,

- $h(\bullet, \alpha_{\mathrm{i}})$ is a non-linear iso-probabilistic transformation that maps a Gaussian scalar variable ($\bullet$) into a *Gamma* distributed one.

- α_{i} are the parameters of $h(\bullet, \alpha_{\mathrm{i}})$ satisfying: $\alpha_{\mathrm{i}} = \frac{7}{2\delta_g^2} - \frac{\mathrm{i}-1}{2}$

The dispersion of the random matrix $\boldsymbol{G}(\delta_g)$ explicitly depends on δ_g (see [28]):

$$\frac{E\left\{\|\boldsymbol{G}(\delta_g) - \mathbf{Id_6}\|^2\right\}}{6} = \delta_g^2 \tag{8}$$

2.1.2 Random isotropic elasticity moduli

As far as random isotropic elasticity moduli are concerned, the bulk and shear moduli have been chosen since they are the eigenvalues of the elasticity tensor (see for instance [16, 5]) and thus lead to a diagonal representation. These moduli are then modeled as independent random variables of strictly positive real value. Applying the maximum entropy principle with given mean values $(\underline{\kappa}, \underline{\mu})$ and mean logarithm, leads to two *Gamma* distributed random variables. In addition, they can be modeled using transforms of 2 independent copies of the Gaussian scalar variable $\mathcal{G}$. It should be noted that, the Gaussian $\mathcal{G}$ is the same as the one constituting the entries of $\boldsymbol{G}$. Hence, by extending the $k-$subscription used in equation (7) beyond $k = 21$, we can write the 2 elasticity moduli as follows:

$$\kappa(\delta) = \delta \underline{\kappa} h(\mathcal{G}_{22}, \delta) \quad \text{and} \quad \mu(\delta) = \delta \underline{\mu} h(\mathcal{G}_{23}, \delta) \tag{9}$$

It is worth noticing that other probability laws such as lognormal could have been chosen, together with correlations between these two gaussian germs.

2.1.3 Properties of matrix-valued random variable C

Thanks to the knowledge of $\kappa(\delta)$, $\mu(\delta)$ and $\boldsymbol{G}(\delta_g)$, the random elastic tensor $\boldsymbol{C}(\delta; \delta_g)$ defined in equation (5) has the following properties (see [30] for more details):

(i) $\boldsymbol{C}(\delta; \delta_g)$ *has an isotropic mean given by:*

$$\underline{C} = 3\underline{\kappa}\boldsymbol{S} + 2\underline{\mu}\boldsymbol{D}, \tag{10}$$

(ii) $\boldsymbol{C}(\delta, \delta_g)$ *is a second order random variable*:

$$E\left\{\|\boldsymbol{C}(\delta, \delta_g)\|_{\mathrm{F}}^2\right\} \leq +\infty \tag{11}$$

(iii) $\boldsymbol{C}^{-1}(\delta, \delta_g)$ *is a second order random variable when* $\delta^2 < \frac{1}{2}$ *and* $\delta_g^2 < \frac{7}{11}$

(iv) *The anisotropy level is linearly controlled by* δ_g:

$$\underline{I}_a = \sqrt{\frac{19}{21}}\delta_g. \tag{12}$$

(v) *The global fluctuation of the norm of* $\boldsymbol{C}(\delta, \delta_g)$ *depends explicitly on* δ_g *and* δ *as:*

$$\delta_{|C|}^2 = \frac{E\left\{\|\boldsymbol{C} - \underline{C}\|_{\mathrm{F}}^2\right\}}{\|\underline{C}\|_{\mathrm{F}}^2} = \delta^2 + \frac{\delta_g^2}{7}\left(1 + \frac{\mathrm{tr}^2(\underline{C})}{\|\underline{C}\|_{\mathrm{F}}^2}\right) \tag{13}$$

Finally, property (v) is obtained using the expression of the 4th-order tensor of covariance of $\boldsymbol{G}(\delta_g)$ given in [28].

REMARK 1 *The anisotropy level that is used at (iv) is based on decomposition (5), and is defined as the mean square distance between* $\boldsymbol{G}(\delta_g)$ *and its projection* $\overline{\boldsymbol{C}}(\delta_g) = (\boldsymbol{S} \otimes \boldsymbol{S} + \boldsymbol{D} \otimes \boldsymbol{D}/5)\boldsymbol{G}(\delta_g)$ *on the isotropic subspace of* $\mathbb{M}_6^+(\mathbb{R})$: *normalized by the square of the norm of the mean value of* $\boldsymbol{G}$:

$$\underline{I}_a = \sqrt{\frac{E\left\{\|\boldsymbol{G} - \overline{\boldsymbol{C}}\|_{\mathrm{F}}^2\right\}}{6}} \tag{14}$$

This anisotropy index is somewhat different from other, more usual definitions [4, 8], based on the distance in the Frobenius norm between the elasticity tensor $\boldsymbol{C}$ and the closest isotropic one $\boldsymbol{C}^{iso}_{eqv}$, defined as $\boldsymbol{C}^{iso}_{eqv} = (\boldsymbol{S} \otimes \boldsymbol{S} + \boldsymbol{D} \otimes \boldsymbol{D}/5)\,\boldsymbol{C}$:

$$I_a = \sqrt{\frac{\|\boldsymbol{C} - \boldsymbol{C}^{iso}_{eqv}\|^2_{\mathrm{F}}}{\|\boldsymbol{C}\|^2_{\mathrm{F}}}}. \tag{15}$$

The analytical relation (12) is a direct consequence of that choice of a definition.

REMARK 2 *When $\underline{I}_a = 0$ the material is almost surely isotropic. When $\delta = 0$, the results on the general random anisotropic tensor given in [28] are retrieved.*

2.2 Stochastic field of elasticity tensor

Up to now, only the variability of the elasticity tensor at a given point has been accounted for. In order to introduce the spatial variability of this mechanical property, the present section discusses the construction of a model of the stochastic field of elasticity tensor based on the probabilistic model developed in the previous section. Let $\boldsymbol{\Omega} = \{\boldsymbol{x}|\boldsymbol{x} \in \mathbb{R}^3\}$ be the physical domain, equipped with a Cartesian reference frame $\{\boldsymbol{i}_1, \boldsymbol{i}_2, \boldsymbol{i}_3\}$, and occupied by an inhomogeneous elastic material. The associated stochastic field model of elasticity tensor $\{\mathbb{C}(\delta; \delta_g; \boldsymbol{\ell})|\boldsymbol{x} \in \boldsymbol{\Omega}\}$, defined on the probability measure space $(\mathcal{A}, \mathcal{F}, P)$, indexed on $\boldsymbol{\Omega}$, with values in $\mathbb{M}^+_6(\mathbb{R})$, can then be formulated as follows:

$$\begin{Bmatrix} \mathbb{C}(\boldsymbol{x}; \delta, \delta_g; \boldsymbol{\ell}) = \left(\sqrt{3\kappa(\boldsymbol{x}; \delta; \boldsymbol{\ell})}\boldsymbol{S} + \sqrt{2\mu(\boldsymbol{x}; \delta; \boldsymbol{\ell})}\boldsymbol{D} \right) \boldsymbol{G}(\boldsymbol{x}; \delta_g; \boldsymbol{\ell}) \\ \left(\sqrt{3\kappa(\boldsymbol{x}; \delta; \boldsymbol{\ell})}\boldsymbol{S} + \sqrt{2\mu(\boldsymbol{x}; \delta; \boldsymbol{\ell})}\boldsymbol{D} \right) \end{Bmatrix} \text{a.s.} \tag{16}$$

where $\boldsymbol{\ell} = (\ell_1, \ell_2, \ell_3)$ is a vector of correlation lengths in the three spatial directions. The evolution from equation (5) to equation (16) is done by replacing, in the formulation of the kernel $\boldsymbol{G}$ and of the isotropic elastic modulus κ, μ, the 23 independent copies $\{\mathcal{G}_{\mathrm{k}}|\mathrm{k} \in \{1, 2, ..., 23\}\}$ of a Gaussian normalized random variable by 23 independent copies $\{\boldsymbol{\mathcal{G}}_{\mathrm{k}}(\boldsymbol{x}; \boldsymbol{\ell})|\boldsymbol{x} \in \boldsymbol{\Omega}; \mathrm{k} \in \{1, 2, ..., 23\}\}$ of a stochastic Gaussian field $\{\boldsymbol{\mathcal{G}}(\boldsymbol{x}; \boldsymbol{\ell})|\boldsymbol{x} \in \boldsymbol{\Omega}\}$ indexed on $\boldsymbol{\Omega}$ with values in $\mathbb{R}$. This germ Gaussian field is of second-order, homogeneous with a correlation structure defined by the following correlation function (see, [29, 3, 24], for more details):

$$R_{\mathcal{G}}(\boldsymbol{\eta}; \boldsymbol{\ell}) = E\left\{ \boldsymbol{\mathcal{G}}(\boldsymbol{x}; \boldsymbol{\ell})\boldsymbol{\mathcal{G}}(\boldsymbol{x} + \boldsymbol{\eta}; \boldsymbol{\ell}) \right\} = \rho(\eta_1, \ell_1)\rho(\eta_2, \ell_2)\rho(\eta_3, \ell_3) \tag{17}$$

where $\rho(\eta; \ell)$ is chosen as a *squared cardinal sine*:

$$\rho(\eta; \ell) = \frac{4\ell^2}{\pi^2\eta^2} \sin^2\left(\frac{\pi\eta}{2\ell}\right) \tag{18}$$

This stochastic field $\{\mathbb{C}(\boldsymbol{x}; \delta, \delta_g; \boldsymbol{\ell})\}$ is mean-square continuous with almost surely continuous samples. Following [29], it can be shown that taking the restriction of this field on a bounded domain leads to a second order solution of the related stochastic boundary value problem.

EXAMPLE 1 *As an example, a soil cube filling the physical domain $\{\boldsymbol{x} \in \boldsymbol{\Omega}_0 \subset \boldsymbol{\Omega}| -200\mathrm{m} \leq x_1, x_2 \leq 200\mathrm{m}; -400\mathrm{m} \leq x_3 \leq 0\mathrm{m}\}$ is considered now. The material has a constant bulk density $\rho_v = 2000\mathrm{kg/m}^3$. The mean model consists in a homogeneous isotropic elastic material with compression wave velocity $v_p = 1730$ m/s and shear wave velocity $v_s = 1000$ m/s. A simulation by the spectral representation approach (see below) is then performed. The mapping of term C_{11} of a sample of the field $\mathbb{C}(\boldsymbol{x}; \delta, \delta_g; \boldsymbol{\ell})$ with $\delta = 0.6\,; \delta_g = 0.15\,; \ell_1 = \ell_2 = 50\mathrm{m}$ and $\ell_3 = 20\mathrm{m}$ is shown in (Figure 1-a). The shorter correlation length along the vertical axis is clearly visible on this chart. In Figure1-b, a good match between the theoretical unidimensional correlation function given by equation (18) and the ones obtained by spatial mean is*

observed. Another remark is that despite the isotropic mean behavior, the elastic tensor is anisotropic almost everywhere. For instance, the elasticity tensor at the point $\{x_1 = x_2 = x_3 = 0\}$ of the given field sample is:

$$C(\mathbf{0}, ...) = \begin{pmatrix} 6.369 & 0.461 & 0.880 & 0.671 & -0.303 & -0.178 \\ - & 3.949 & 1.403 & 0.039 & -0.405 & -0.513 \\ - & - & 4.394 & -0.142 & -0.152 & -0.662 \\ - & - & - & 3.091 & -1.072 & -0.081 \\ - & (sym.) & - & - & 2.036 & 0.224 \\ - & - & - & - & - & 2.047 \end{pmatrix} [\times 10^9 \mathrm{Pa}] \qquad (19)$$

(a)　　　　　　　　　　(b)

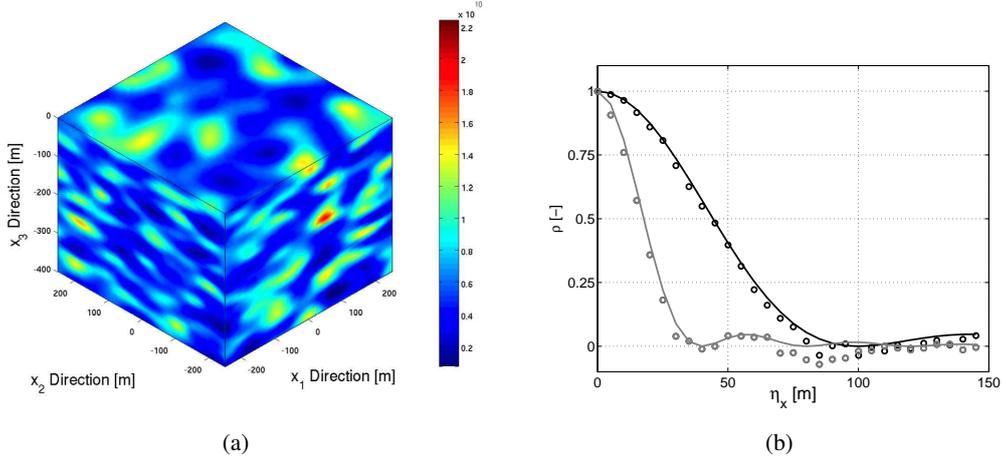Figure 1: A sample of stochastic elasticity tensor field: (a) Mapping of C_{11}. (b) Theoretical (solid lines) and observed (circles) correlation structures in $\mathbf{i}_1-$ (black) and $\mathbf{i}_3-$ (gray) directions.

We now consider two samples of a random media having the same: mean homogeneous isotropic elastic properties, fluctuation level $\delta_{|C|}$ and correlation length vector $\boldsymbol{\ell}$, but different values for the dispersion parameters δ and δ_g in order to observe the influence of these parameters on the wave propagation pattern.

EXAMPLE 2 *The domain of interest is such that $-1500\mathrm{m} \leq x_1, x_2 \leq 1500\mathrm{m}$ and $-400\mathrm{m} \leq x_3 \leq 0\mathrm{m}$. The mean wave velocities are $v_\mathrm{p} = 1730\mathrm{m/s}$ and $v_\mathrm{s} = 1000\mathrm{m/s}$. Free surface boundary conditions are applied on top $x_3 = 0$ and PML conditions on the other sides of the box. A point source is located at point $\boldsymbol{x}_o = (-1400, 0, 0)$ on the free surface. The time history of the force is a Ricker with a characteristic frequency equal to $10\mathrm{Hz}$. The three correlation lengths are equal to $100\mathrm{m}$. As a consequence, the dominant wavelength is of the order of the correlation length and the domain characteristic size is about ten times the wavelength. As far as the amplitude of the fluctuation is concerned, the global fluctuation level on the elastic tensor is set to $\delta_{|C|} = 0.49$. The dispersion parameters are set to $\delta = 0; \delta_g = 0.6$ for the first model, which corresponds to the original model proposed in [29]. These parameters are set to $\delta = 0.47; \delta_g = 0.17$ for the second model which corresponds to the upper limit of the anisotropic index observed in geophysics [32]. The amplitudes of the particle velocity on the free surface are shown in (Figure 2) for three different time steps and for the two models. Although $\delta_{|C|}$ is the same in the two cases, the wave propagation patterns are very different. In the case of a high anisotropic level ($\delta_g = 0.6$) the diffusion pattern corresponds to a strong diffusion of the wave field whereas in the weakly anisotropic case ($\delta_g = 0.17$) the wave field seems much more localized in space and in time. Scattering at given locations can be observed. These results indicate that these two models lead to different propagation regimes which have to be charaterized in more details.*
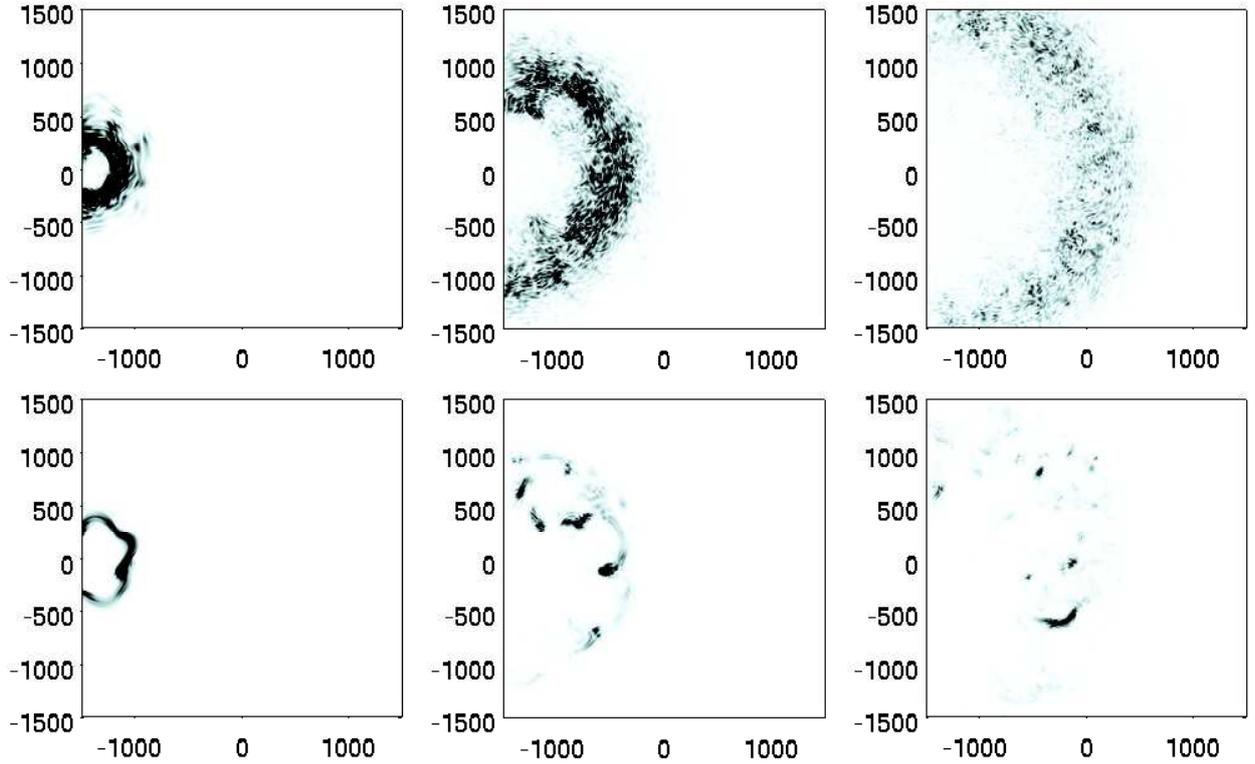
Figure 2: Time evolution (from left to right) of wavefronts on the free surface for $\delta_{|C|} = 0.49$: (upper figures) $\delta = 0$; $\delta_g = 0.6$, (lower figures) $\delta = 0.47$; $\delta_g = 0.17$.

2.3 Generation of a realization of the stochastic field of elasticity tensor

We address here the issue of generating a sample of the random field of elasticity tensor. As we wish to propagate the waves over large distances, we are required to use a cluster of computers with distributed memory. Further, in the case that interests us, the correlation length is of the order of magnitude of the wavelength, which controls the size of the finite elements, for accuracy reasons. Hence, the elasticity tensor evolves significantly over the size of an element, and it has to be sampled at all Gauss-Lobatto-Legendre points. As an example, the number of space points at which the elasticity tensor is sampled is of the order of magnitude of several tens of millions (for run presented in Figure 2). This means an order of magnitude of 10^9 values to be computed and stored (21 coefficients per space points).

The main goal of such an operation over a cluster with distributed memory consists in performing as much work as possible over each thread independently, while retaining the global continuity of the elasticity tensor (see Figure 3). We chose here to use the spectral representation method (see, [27], for instance). For this method, and when using a homogeneous grid (all machines are the same), only the seed of the pseudo-random generator has to exchanged between the threads (for example, through the main parameter file). When using a heterogeneous grid, the values of the random germs (the size of which is usually much smaller than 10^9) have to be exchanged.

More specifically, each thread executes, only over its own space domain, and for each of the 23 germs $\{\boldsymbol{\mathcal{G}}_k(\boldsymbol{x}; \boldsymbol{\lambda}_c) \,|\, 1 \leq k \leq 23\}$, the following formula:

$$\boldsymbol{\mathcal{G}}_k(\boldsymbol{x}; \lambda_1^c, \lambda_2^c, \lambda_3^c) = \sqrt{2 \frac{\pi}{\lambda_1} \frac{\pi}{\lambda_2} \frac{\pi}{\lambda_3}} \sum_{\boldsymbol{\kappa} \in \text{support} \boldsymbol{H}^{\mathcal{G}}} \sqrt{H_1^{\mathcal{G}} H_2^{\mathcal{G}} H_3^{\mathcal{G}}} \, \mathbb{Y}(\boldsymbol{\kappa}|a) \cos(2\pi \mathbb{Z}(\boldsymbol{\kappa}|a) + \boldsymbol{\kappa} \cdot \boldsymbol{x}), \qquad (20)$$

where the $H_i^{\mathcal{G}}$ are related to the Fourier spectrum of the correlation structure $\rho(\eta; \ell)$ chosen for the random
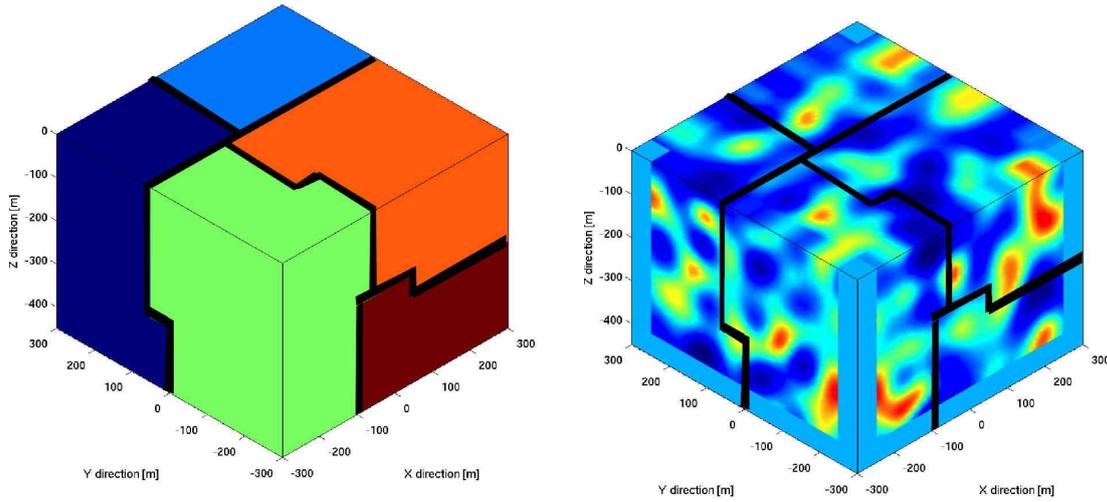
Figure 3: Example of fields generated by sub-domains (one sub-domain per thread): geometry of the sub-domains (left figure) and one realization of the component C_{44} of the elasticity tensor (right figure).

field of elasticity tensor, and the a emphasize the quantity that has to be exchanged, depending on the heterogeneity of the cluster over which the computation is run. Note that these sums can be very efficiently implemented and computed using the Fast Fourier Transform, for which parallel implementations exist on large clusters.

3 Boundary conditions: PMLs

We consider in this section the truncation of the space domain over which the computation is run. Indeed, in homogeneous media, it has become quite common to use either absorbing boundaries or layers to reduce the size of the domain over which the computation is run. Both these general approaches (that incorporate many different methods) aim at absorbing the outgoing waves through the imposition of a particular boundary condition (absorbing boundaries) or by the addition of some absorbing material around the computational domain (absorbing layers). When schemes have shown to behave very well. In particular, the Perfectly Matched Layer method [7] has taken a place of choice for applications in electromagnetism [31, 10], acoustics [20] and elastodynamics [15, 11, 18, 13].

However, in a heterogeneous domain, some energy might be reflected inside the computational domain by a heterogeneity located outside of it. Hence the absorption of the outgoing waves actually decreases the energy inside the computational domain. The development of equivalent boundary conditions in such media is still a pending question to the authors' knowledge, and will not considered here. In this section we describe, respectively, the implementation of the PMLs for elastodynamics, the instability arising in heterogeneous anisotropic media, and a possible patch for that problem.

3.1 PMLs in elastodynamics

The absorbing property of the PML is represented mathematically by the modification of the divergence operator in the strong formulation of the elastodynamics equation:

$$\widetilde{Div}\boldsymbol{\sigma} + \boldsymbol{f_v} = \rho_v \ddot{\boldsymbol{u}}. \tag{21}$$
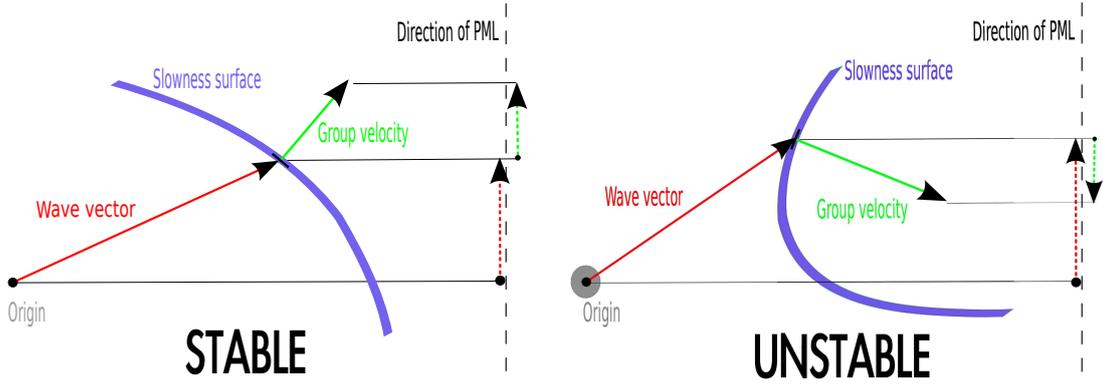
Figure 4: Instability issue with PMLs in anisotropic medium.

This modified divergence operator $\widetilde{Div}$ is written

$$\widetilde{Div} = \frac{1}{S_x}\boldsymbol{e}_x\partial x + \frac{1}{S_y}\boldsymbol{e}_y\partial y + \frac{1}{S_z}\boldsymbol{e}_z\partial z, \tag{22}$$

with S_i the stretching function along the direction $\boldsymbol{e}_i$. As in [14] for the simplest case of a boundary of normal $\boldsymbol{n}_j$, this function can be chosen in the frequency domain as:

$$S_i = 1 - i\frac{\beta_i(x_i)}{\omega}\delta_{ij}, \tag{23}$$

with δ_{ij} the Kronecker symbol and $\beta_i(x_i)$ a real function of the distance to the interface between the physical and absorbing domains. This function is chosen strictly positive and starting at zero to ensure the continuity of the material at the interface.

The modified divergence operator $\widetilde{Div}$ can also be seen as a change of coordinates

$$\widetilde{x}_i = x_i - \frac{i}{\omega}\int_0^{x_i}\beta_i(s)ds. \tag{24}$$

Physically the modified divergence operator implies that there is an exponential attenuation within the PMLs. Indeed a PML region perpendicular to $\boldsymbol{e}_x$ transforms (see [11], for instance) a plane wave

$$\Phi(x,y,z,t) = \boldsymbol{\Phi}_0 e^{i(\omega t - k_x x - k_y y - k_z z)} \tag{25}$$

into the wave

$$\widetilde{\Phi}(x,y,z,t) = \boldsymbol{\Phi}_0 e^{i(\omega t - k_x x - k_y y - k_z z)}e^{-\frac{k_x}{\omega}\int_0^x \beta_x(s)ds} \tag{26}$$

which has been attenuated by a factor of $e^{-\frac{k_x}{\omega}\int_0^x \beta_x(s)ds}$.

3.2 Instability of PMLs in heterogeneous anisotropic media

Although PMLs behave very well, it has been shown that they become unstable, in the case of anisotropic media, for certain relations of the group velocity and the orientation of the layer [6] (see Figure 4). Unfortunately, this situation always occurs when considering heterogeneous and anisotropic media. This section describes this instability.

For elastic waves, there are two equivalent ways to implement the PMLs: by decomposing waves into potential energies of compression and shear, as in [15], or through a stress-velocity formulation, as in most

application in elastodynamics [14]. This approach is followed here, and the system of equations to be solved is:

$$\begin{cases} \rho_v(\dot{v}_i^m + \beta_m v_i^m) = \dfrac{\partial \sigma_{ij}}{\partial x_j}\boldsymbol{\delta}_{jm} \\[3mm] \dot{\sigma}_{ij}^m + \beta_m \sigma_{ij}^m = C_{ijkl}\dfrac{\partial v_k}{\partial x_l}\boldsymbol{\delta}_{lm} \end{cases} \tag{27}$$

To simplify the notations, and understand the concepts, we choose a PML perpendicular to $\boldsymbol{i}_1$ (*i.e.* the damping in the PML is activated only along the direction $\boldsymbol{i}_1$: $\beta_1 \neq 0$):

$$\begin{cases} \rho_v(\dot{v}_i^m + \boldsymbol{\delta}_{1m}\beta_m v_i^m) = \dfrac{\partial \sigma_{ij}}{\partial x_j}\boldsymbol{\delta}_{jm} \\[3mm] \dot{\sigma}_{ij}^m + \boldsymbol{\delta}_{1m}\beta_m \sigma_{ij}^m = C_{ijkl}\dfrac{\partial v_k}{\partial x_l}\boldsymbol{\delta}_{lm} \end{cases} \tag{28}$$

The system (28) can be assembled in the form of the first-order differential equation:

$$\dot{\boldsymbol{\Psi}} = \boldsymbol{A}_1\frac{\partial \boldsymbol{\Psi}}{\partial x_1} + \boldsymbol{A}_2\frac{\partial \boldsymbol{\Psi}}{\partial x_2} + \boldsymbol{A}_3\frac{\partial \boldsymbol{\Psi}}{\partial x_3} - \boldsymbol{B}\boldsymbol{\Psi} \tag{29}$$

where $\boldsymbol{\Psi}$ is a 27-components-vector

$$\begin{aligned} \boldsymbol{\Psi} = \Big[& \sigma_{11}^{(1)}\ \sigma_{22}^{(1)}\ \sigma_{33}^{(1)}\ \sigma_{12}^{(1)}\ \sigma_{13}^{(1)}\ \sigma_{23}^{(1)}\ v_1^{(1)}\ v_2^{(1)}\ v_3^{(1)}... \\ & \sigma_{11}^{(2)}\ \sigma_{22}^{(2)}\ \sigma_{33}^{(2)}\ \sigma_{12}^{(2)}\ \sigma_{13}^{(2)}\ \sigma_{23}^{(2)}\ v_1^{(2)}\ v_2^{(1)}\ v_3^{(2)}... \\ & \sigma_{11}^{(3)}\ \sigma_{22}^{(3)}\ \sigma_{33}^{(3)}\ \sigma_{12}^{(3)}\ \sigma_{13}^{(3)}\ \sigma_{23}^{(3)}\ v_1^{(3)}\ v_2^{(3)}\ v_3^{(3)} \Big]^{\text{T}} \end{aligned} \tag{30}$$

$\boldsymbol{A}_1, \boldsymbol{A}_2, \boldsymbol{A}_3$ are matrices depending on the mechanical properties C_{ijkl} and ρ_v, and $\boldsymbol{B}$ is a diagonal matrix characterizing the absorbing property of the PML:

$$\boldsymbol{B} = \begin{bmatrix} \beta_1 \mathbf{Id}_9 & \mathbf{0}_{18} \\ \mathbf{0}_{18} & \mathbf{0}_{18} \end{bmatrix}. \tag{31}$$

The equation (29) is associated to a hyperbolic equation that describes the physical domain:

$$\dot{\boldsymbol{\Psi}} = \boldsymbol{A}_1\frac{\partial \boldsymbol{\Psi}}{\partial x_1} + \boldsymbol{A}_2\frac{\partial \boldsymbol{\Psi}}{\partial x_2} + \boldsymbol{A}_3\frac{\partial \boldsymbol{\Psi}}{\partial x_3} \tag{32}$$

and accepts plane wave solutions $\boldsymbol{\Psi}_0 e^{i(\omega t - \boldsymbol{\kappa}\cdot\boldsymbol{x})}$ when $(\boldsymbol{\kappa}, \omega)$ satisfy the dispersion relation:

$$F(\omega, \boldsymbol{\kappa}) = F(\omega, \kappa_1, \kappa_2, \kappa_3) = \det(\omega\mathbf{Id} - \kappa_1\boldsymbol{A}_1 - \kappa_2\boldsymbol{A}_2 - \kappa_3\boldsymbol{A}_3) = 0. \tag{33}$$

Coming back to system (29), it accepts plane wave solutions when the following dispersion relation is met:

$$F^{pml}(\omega, \boldsymbol{\kappa}) = F(\omega, \kappa_1^{pml}, \kappa_2, \kappa_3) = F\left(\omega, \kappa_1\frac{\omega}{\omega - i\beta_1}, \kappa_2, \kappa_3\right) = 0 \tag{34}$$

$$F\Big(\omega(\omega - i\beta_1), \kappa_1(\omega), \kappa_2(\omega - i\beta_1), \kappa_3(\omega - i\beta_1)\Big) = 0 \tag{35}$$

Following [6], the solutions $\boldsymbol{\Psi}$ are stable when the imaginary part of ω is positive. This implies that:

$$\boldsymbol{s} \cdot \boldsymbol{v}_g > 0. \tag{36}$$

Geometrically, the condition (36) implies that the instability of the PML occurs almost surely for long times if the slowness surfaces of the material shows at least one concave part towards the PML. A schematic view of that interpretation is presented in Figure 4.
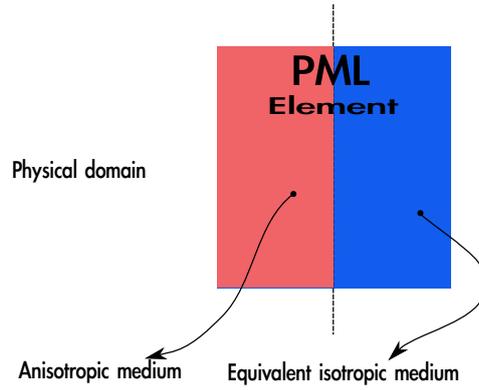
Figure 5: Schematic presentation of the introduction of the isotropic equivalent material in the PML.

3.3 Modified (stable) PMLs for heterogeneous anisotropic media

We present here a modified version of the PMLs that remains stable and reflects very little energy in the case of heterogenous and anisotropic media. Another option consists in using a multiaxial damping [12], which stabilizes the PMLs, but this creates some undesired reflection at the interface between the physical and absorbing domains.

From the geometrical interpretation of the instability issue in the previous section, one remark can be drawn right away: an isotropic material is naturally stable with respect to the PML because the slowness surfaces are spheres. Therefore we will adapt the PML by considering an isotropic equivalent material instead of the original anisotropic material. This isotropic equivalent material is defined as the projection of the elasticity tensor over the space generated by the spherical and deviatoric tensors (see section 2). However, to limit the influence of the loss of "perfect match" between the physical domain and the PML, we only introduce this isotropic equivalent material at some distance from the interface (see Figure 5). The effect of this modification is hence a reduction of the instability issue (in practice, the energy explodes at later times) while keeping the undesired reflections at low levels.

EXAMPLE 3 *We then present a study of the influence of the relative size of the modified PML on the evolution of the total energy inside the physical domain (Figure 6). Let us consider a cube of inhomogeneous soil modeled by a 3D-stochastic anisotropic elasticity tensor field of isotropic mean model (represented by the P-speed and S-speed respectively equal to 1730 $\mathrm{m/s}$ and 1000 $\mathrm{m/s}$). δ and δ_g are chosen such that the whole fluctuation $\delta_{|C|}$ is equal to 50% of the mean. The three correlation lengths are all taken equal to 50m. This physical domain of size 500m $\times$ 500m $\times$ 450m is almost surrounded by 50m-layer-PMLs except for the top side where a free surface boundary condition is applied. Both of these domains (i.e. physical and absorbing) are discretized in hexahedral spectral finite elements of size 50m $\times$ 50m $\times$ 50m. A GLL-grid of order 8 is used for local collocation points. The relative size of the modified PML layer is evaluated in number of GLL points at which the anisotropy behavior is replaced by a isotropic equivalent one. A Ricker point-like source is located at the center of the free surface. 7 random simulations corresponding to these PML configurations are then performed in which the physical domain sample is unchanged from one to another. We observe that in average, the larger the isotropic domain, the further in time the explosion time is sent. Note, however, that this property is not necessarily true for each sample independently because the media that we are considering are realizations of a random medium.*
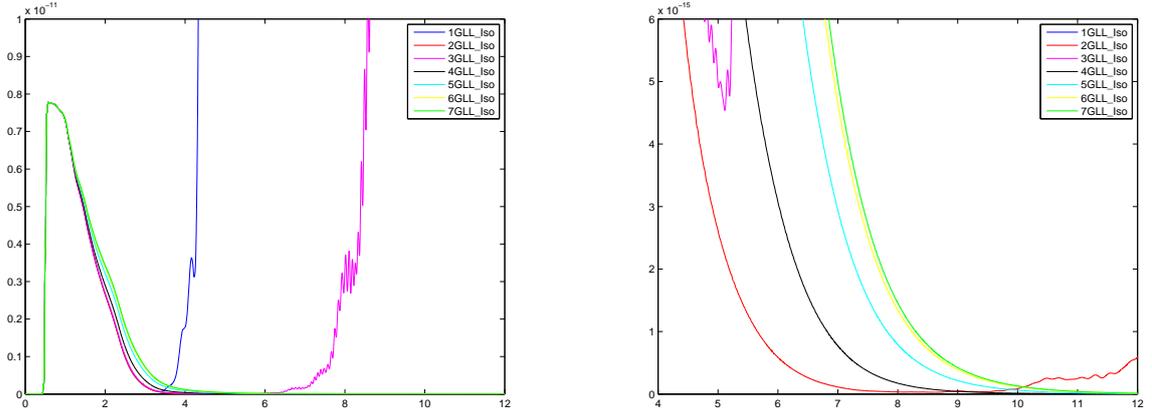
Figure 6: Influence of the relative size of the modified PML on the evolution of the total energy inside the physical domain. The right figure is a (strong) zoom on the left figure.

4   Wave propagation vs. diffusion

In this section, we discuss very briefly a first step in a new direction of research for the observation of wave propagation in random media over long distances. The general motto is that, in some cases, the observation of the velocity field at long distances is not meaningful, and that the observation of energy levels is more important. This is obvious in Figure 2 where a diffusion behavior is observed on the upper graphs. An interesting approach would therefore consist in solving, for long distances, an equation of diffusion for the energy (the coefficients of which can be derived theoretically [25]), rather than the wave equation for the velocity field. The former would require much less computational power because its features are much smoother. Besides the construction of the appropriate coefficients for the diffusion equation, this research direction would require the construction of appropriate excitation given the real excitations of the wave equation. In the longer run, two interesting options would be to couple wave propagation with diffusion some distance away from the excitation, and/or to construct new types of PMLs, that would allow to launch back at the computational domain the appropriate energy, based on the diffusion equation. This last point would address the unsolved problem of PML for heterogeneous media, hinted at in section 3.

The first point of that research program, which is the only one that we will consider here, consists in identifying the emergence of diffusion of energy within the framework of the wave equation. In particular, several authors [23, 22, 19] have shown that diffusion of energy is necessarily accompanied by an equipartition of the compressional wave energy

$$\mathcal{E}_\mathrm{P} = \rho_v v_\mathrm{P}^2 \times \mathsf{E}\left\{ \left(\mathrm{Div}\,\boldsymbol{u} \right)^2 \right\} \tag{37}$$

and the shear wave energy

$$\mathcal{E}_\mathrm{S} = \rho_v v_\mathrm{S}^2 \times \mathsf{E}\left\{ \left(\overrightarrow{\mathrm{Rot}}\,\boldsymbol{u} \right)^2 \right\} \tag{38}$$

of the form

$$\frac{\mathcal{E}_\mathrm{P}}{\mathcal{E}_\mathrm{S}} = \frac{v_\mathrm{P}^3}{2v_\mathrm{S}^3}. \tag{39}$$

Indeed, this equipartition can be observed in the simulations that we have performed. However, this equipartition appears after long distances of propagation, and at long times, so that some work still has to be performed in lowering the computational cost of the solution of the full wave propagation equation over long distances. The main issue with this characterization of diffusion in that manner is that the definition of the compressional wave and shear wave energies is not well defined for anisotropic media. In the example below, we show that the convergence does take place towards the expected value for both isotropic and mildly
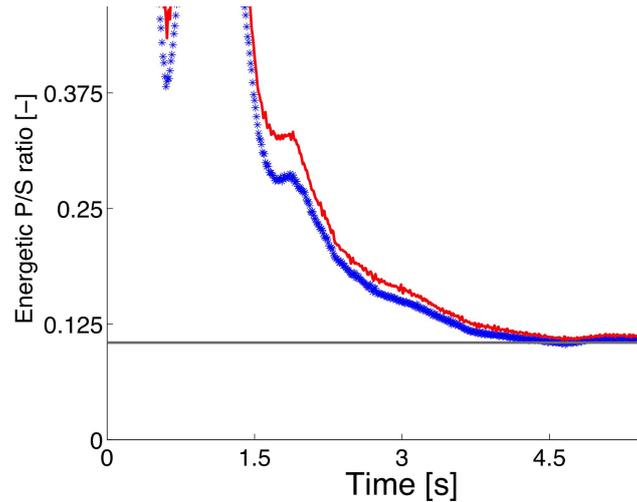
Figure 7: Observation of the equipartition of energy at the theoretical level over long distances of propagation and time for an isotropic model (blue stars) and a mildly anisotropic one (red line).

anisotropic media. However, for more strongly anisotropic media, the convergence does take place but leads to a different value of the ratio of energies. Further investigations are required on that topic.

EXAMPLE 4 *We consider here two different cubes of dimensions* $3000\text{m} \times 3000\text{m} \times 450\text{m}$ *with heterogeneous materials with global variability* $\delta_{|C|} = 0.1$ *and correlation lengths in all directions 100 m. The material of the first is isotropic, with* $\delta = 0.1$ *and* $\delta_g = 0$ *and that of the second one is anisotropic with* $\delta = 0$ *and* $\delta_g = 0.1374$. *In both cases, the domains are discretized in hexahedral spectral finite elements of size* $50\text{m} \times 50\text{m} \times 50\text{m}$. *A GLL-grid of order 8 is used for local collocation points. In both cases, no PMLs are implemented and Neumann boundary conditions are used all over. This is done so as to contaminate the energy inside the domain through undesired reflections and/or undesired loss. On Figure 7, the convergence of the ratio of the energies towards the expected value can be observed.*

References

[1] M. Ainsworth, H. A. Wajid, *Dispersive and dissipative behavior of the spectral element method*, SIAM Journal of Numerical Analysis, Vol. 47, No. 5 (2009), pp. 3910-3937.

[2] K. Aki and B. Chouet, *Origin of coda waves: source, attenuation and scattering effects*, Journal of Geophysical Research, Vol. 80, No. 23 (1975), pp. 3322-3342.

[3] M. Arnst, D. Clouteau, M. Bonnet, *Inversion of probabilistic structural models using measured transfer functions*, Computer Methods in Applied Mechanics and Engineering, Vol. 197, No. 6-8 (2008), pp. 589-608.

[4] R. J. Arts, *Étude de l'élasticité anisotrope générale dans les roches par propagation de sondes*, PhD thesis, Université Pierre et Marie Curie, Paris, France (1993).

[5] P. Basser, S. Pajevic, *Spectral decomposition of a 4th-order covariance tensor*, Signal Processing, Vol. 87 (2007), pp. 220-236.

[6] E. Bécache, S. Fauqueux, P. Joly, *Stability of perfectly matched layers, groups velocities and anisotropic waves*, Journal of Computational Physics, Vol. 188 (2003), pp. 399-433.

[7] F. Bérenger, *A perfectly matched layer for the absorption of electromagnetics waves*, Journal of Computational Physics, Vol. 114 (1994), pp. 185-200.

[8] J.-M. Carcione, *Wave fields in real media: wave propagation in anisotropic, anelastic, porous and eletromagnetic media*, Vol. 38 of Handbook of Geophysical Exploration: Seismic Exploration, Elsevier (2007).

[9] D. Clouteau, D. Aubry, *Modification of the ground motion in dense urban areas*, Computational Acoustics, Vol. 9, No. 4 (2001), pp. 1659-1675.

[10] F. Collino and P. Monk, *The perfectly matched layer in curvilinear corrdinates*, SIAM Journal on Numerical Analysis, Vol. 19, No. 6 (1998), pp. 2061-2090.

[11] A. Collino, C. Tsogka, *Application of the PML absorbing layer model to the linear elastodynamic problem in anisotropic heterogeneous media*, Geophysics, Vol. 66, No. 1 (2000), pp. 294-307.

[12] K. Meza-Fajardo, A. Papageorgiou, *A nonconvolutional, split-field, perfectly matched layer for wave propagation in isotropic and anisotropic elastic media: stability analysis*, Bulletin of the Seismological Society of America, Vol. 98, No. 4 (2008), pp. 1811-1836.

[13] G. Festa, *Slip imaging by isochron back projection and source dynamics with spectral element methods*, PhD thesis, Unisversità degli studi di Bologna, Bologna, Italy (2004).

[14] G. Festa, J.-P. Vilotte, *The Newmark scheme as a velocity-stress time staggering: an efficient PML for spectral element simulations of elastodynamics*, Geophysical Journal International, Vol. 161, No. 3 (2005), pp. 789-812.

[15] F. D. Hastings, J. B. Schneider, S. L. Broschat, *Application of the perfectly matched layer (PML) absorbing boundary condition to elastic wave propagation*, Journal of the Acoustical Society of America, Vol. 100, No. 5 (1996), pp. 3061-3069.

[16] K. Helbig, *Foundations of anisotropy for exploration seismics*, Elsevier (1994).

[17] E. T. Jaynes, *Information theory and statistical mechanics*, Physical Review, Vol. 106, No. 4 (1957), pp. 620-630.

[18] D. Komatitsch, J. Tromp, *A perfectly matched layer absorbing boundary condition for the second order seismic wave equation*, Geophysical Journal International, Vol. 154 (2003), pp. 146-153.

[19] E. Larose, *Diffusion multiple des ondes sismiques et expériences analogiques en ultrasons*, PhD thesis, Université Joseph Fourier, Grenoble, France (2003).

[20] Q. H. Liu, J. Tao, *The perfectly matched layer (PML) for acoustic waves in absorptive media*, Journal of the Acoustical Society of America, Vol. 102 (1997), pp. 2072-2082.

[21] L. Margerin, *Diffusion multiple des ondes élastiques dans la lithosphère*, PhD thesis, Université Joseph Fourier, Grenoble, France (1998).

[22] L. Margerin, M. Campillo, B. V. Tiggelen, *Monte Carlo simulation of multiple scattering of elastic waves*, Journal of Geophysical Research, Vol. 105, No. B4 (2055), pp. 7873-7892.

[23] G. C. Papanicolaou, L. V. Ryzhik, J. B. Keller, *Stability of the P-to-S energy ratio in the diffusive regime*, Bulletin of the Seismological Society of America, Vol. 86 (1996), pp. 1107-1115.

[24] R. Popescu, *Stochastic variability of soil properties: data analysis, digital simulation, effect on system behavior*, PhD thesis, Princeton University, USA (1995).

[25] L. V. Ryzhik, G. C. Papanicolaou, J. B. Keller, *Transport equations for elastic and other waves in random media*, Wave Motion, Vol. 24 (1996), pp. 327-370.

[26] C. E. Shannon, *A mathematical theory of communication*, The Bell System Technical Journal, Vol. 27 (1948), pp. 379–423, 623–656.

[27] M. Shinozuka, G. Deodatis, *Simulation of multi-dimensional Gaussian stochastic fields by spectral representation*, Applied Mechanics Review, Vol. 1, No. 49 (1996), pp. 29-53.

[28] C. Soize, *Random matrix theory for modeling uncertainties in computational mechanics*, Computer Methods in Applied Mechanics and Engineering, Vol. 194 (2005), pp. 1333-1366.

[29] C. Soize, *Non-gaussian positive-definite matrix-valued random fields for elliptic stochastic partial differential operators*, Computer Methods in Applied Mechanics and Engineering, Vol. 195, No. 1-3 (2006), pp. 26-64.

[30] Q.-A. Ta, D. Clouteau, R. Cottereau, *Modeling of random anisotropic elastic media and impact on wave propagation*, European Journal of Computational Mechanics, Vol. 19, No. 1-3 (2010), pp. 241-253.

[31] F. L. Teixera and W. C. Chew, *Systematic derivation of anisotropic PML absorbing media in cylindrical and spherical coordinates*, IEEE Microwave and Guided Wave Letters, Vol. 7, No. 11 (1997), pp. 371-374.

[32] L. Vernik, X. Liu, *Velocity anisotropy in shales: a petrophysical study*, Geophysics, Vol. 62 (1997), pp. 521-532.